Journal Pre-proofs

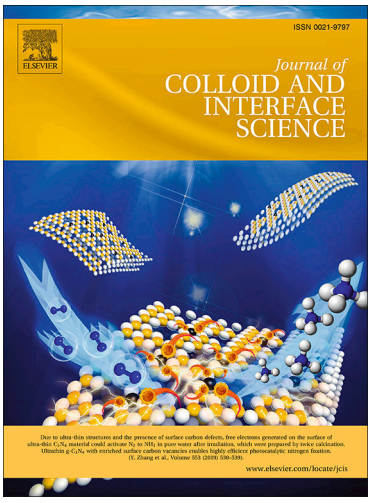


Regular Article

# Spin diffusion transfer difference (SDTD) NMR: an advanced method for the characterisation of water structuration within particle networks

Valeria Gabrielli, Agne Kuraite, Marcelo Alves da Silva, Karen J. Edler, Jesús Angulo, Ridvan Nepravishta, Juan C. Muñoz–García, Yaroslav Z. Khimyak

PII: S0021-9797(21)00246-0
DOI: https://doi.org/10.1016/j.jcis.2021.02.094
Reference: YJCIS 27638

To appear in: *Journal of Colloid and Interface Science*

Received Date: 20 November 2020
Revised Date: 13 February 2021
Accepted Date: 23 February 2021

Please cite this article as: V. Gabrielli, A. Kuraite, M. Alves da Silva, K.J. Edler, J. Angulo, R. Nepravishta, J.C. Muñoz–García, Y.Z. Khimyak, Spin diffusion transfer difference (SDTD) NMR: an advanced method for the characterisation of water structuration within particle networks, *Journal of Colloid and Interface Science* (2021), doi: https://doi.org/10.1016/j.jcis.2021.02.094

# Spin diffusion transfer difference (SDTD) NMR: an advanced method for the characterisation of water structuration within particle networks

Valeria Gabrielli,[a] Agne Kuraite,[a] Marcelo Alves da Silva,[b] Karen J. Edler,[b] Jesús Angulo,[a,c] Ridvan Nepravishta,[a,d]* Juan C. Muñoz-García[a]* and Yaroslav Z. Khimyak[a]*

[a] School of Pharmacy, University of East Anglia, Norwich Research Park, Norwich, NR4 7TJ, UK.

[b] Department of Chemistry, University of Bath, Claverton Down, Bath, BA2 7AY, UK.

[c] Present address: Department of Chemistry, University of Sevilla, Professor García González St, Sevilla, 41012, Spain

[d] Present address: Department of Biochemistry and Molecular Biology, The University of Texas Medical Branch, Galveston, TX 77555, United States

* Corresponding authors: y.khimyak@uea.ac.uk; j.munoz-garcia@uea.ac.uk; rineprav@utmb.edu

## Abstract

Hypothesis

The classical STD NMR protocol to monitor water interactions in gels is strongly dependent on gelator and solvent concentrations and does not report on the degree of structuration of the solvent at the particle/solvent interface. We hypothesised that, for suspensions of large gelator particles, solvent structuration could be characterised by STD NMR when taking into account the particle-to-solvent $^{1}H$-$^{1}H$ spin diffusion transfer using the 1D diffusion equation.

Experiments

We have carried out a systematic study on effect of gelator and solvent concentrations, and gelator surface charge, affecting the behaviour of the classical STD NMR build-up curves. To do so, we have characterised solvent interactions in dispersions of starch and cellulose-like particles prepared in deuterated water and alcohol/$D_2O$ mixtures.

Findings

The Spin Diffusion Transfer Difference (SDTD) NMR protocol is independent of the gelator and solvent concentrations, hence allowing the estimation of the degree of solvent structuration within different particle networks. In addition, the simulation of SDTD build-up curves using the general one-dimensional diffusion equation allows the determination of minimum distances (*r*) and spin diffusion rates (*D*) at the particle/solvent interface. This novel NMR protocol can be readily extended to characterise the solvent(s) organisation in any type of colloidal systems constituted by large particles.

**Abbreviations**: SDTD, Spin Diffusion Transfer Difference; NOE, Nuclear Overhauser Effect; erfc, complementary error function; OCNF, Oxidised Cellulose Nanofibrils

**Keywords**: spin diffusion, saturation transfer difference NMR, hydrogel, solvation properties

## 1. Introduction

The phenomenon of spin diffusion can be generally described as the transfer of magnetisation through space via "flip-flop" mechanism.[1] Briefly, considering two dipolar coupled spin-1/2 nuclei tumbling isotropically in solution, magnetisation exchange or cross-relaxation can (i) occur spontaneously when the αβ and βα energy levels have the same energy (equivalent spins) and, therefore, the mechanism of cross-relaxation is energy conserving (†ESI, Figure S1a),[2] and (ii) occur with low probability when the two spins are not equivalent (most common case) and, hence, the exchange of magnetisation is non-energy-conserving (†ESI, Figure S1b).[2] Both of these phenomena are the basis of the well-known Nuclear Overhauser Effect (NOE), a key building block in many solution NMR experiments. In other words, in liquids the cross-relaxation (*i.e.* NOE) induced by the molecular motion modulation of dipolar couplings is responsible for the transfer of magnetisation between spin pairs close in space (within *ca.* 5 Å).

On the contrary, in solids the strong homonuclear dipolar couplings between abundant and spatially fixed spins (anisotropic samples) give rise to splitting (broadening) of the energy levels of the two-spin system, as each pair of inequivalent spins are dipolar coupled to many others. As a consequence, the increased number of equivalent αβ and βα states boosts the probability of energy-conserving magnetisation exchange (†ESI, Figure S1c).[2] This enhancement is generally called *spin diffusion* within the solid-state NMR community. This

solids-linked phenomenon is not related to molecular motion but to a coherent effect due to incomplete MAS averaging of the $^{1}$H-$^{1}$H dipolar interactions.[3,4] For this reason, NOE-based solid-state NMR pulse sequences are often referred to as spin diffusion experiments because the dominant mechanism of magnetisation transfer in solids is spin diffusion. To avoid confusion, both definitions of spin diffusion are usually classified as coherent spin diffusion (solids) and incoherent spin diffusion (liquids). In semisolid samples (*e.g*. gels), both coherent and incoherent spin diffusion can play a role, although the contribution of coherent spin diffusion is expected to be much larger than the incoherent mechanism (reduced efficiency of magnetization transfer). In this work, when we use the term *spin diffusion* we will be referring to coherent spin diffusion.

For macromolecules in solution undergoing Brownian motion, STD NMR relies on the selective saturation of receptor signals followed by intramolecular NOE between dipolar coupled protons. This leads to the transfer of saturation to the entire macromolecule and, subsequently, to the transfer of magnetisation to fast-exchanging binders by intermolecular NOE. However, for large systems such as the tens of nm to µm long particles constituting a gel, spin diffusion is boosted due to the presence of very strong $^{1}$H-$^{1}$H dipolar couplings. Previous experiments on membrane proteins and plant cell walls (PCWs) demonstrated that the mechanism of spin diffusion is not limited to magnetisation exchange within and between large particles, but also applies to magnetisation transfer from the particles (e.g. PCW particle network, membrane protein) to the small mobile components (*e.g*. water, lipids).[5–8] Thus, spin-diffusion-based NMR methods such as the water polarisation transfer solid-state NMR experiment allows monitoring the $^{1}$H magnetisation transfer from a mobile to a rigid component *via* chemical exchange and spin diffusion (during a mixing time), followed by $^{13}$C detection *via* cross polarisation (CP).[5,6] By applying increasing mixing times, the build-up curve of the mobile-to-rigid magnetisation transfer is obtained. To fit the spin diffusion build-up curve several equations based on the diffusion equation have been proposed,[9,10] the 1D diffusion equation being the most commonly employed (Eq. 1; see †ESI for mathematical demonstration):

$$I = C \cdot erfc\left[\frac{r}{2 \cdot \sqrt{D \cdot t}} - b\right] \qquad \textit{Eq. 1}$$

where *I* is the normalised intensity of the peak, the independent variable (*t*) is the square root of mixing time (in ms$^{1/2}$), C is the proportionally constant of the fit, *erfc* is the complementary

error function, *r* is the minimum distance of the grid (in nm), *D* is the spin diffusion rate (in $nm^2/ms$), and *b* is a mathematical parameter to centre the error function around 0. Importantly, while the slope of the curve is determined mainly by the diffusion rate *D* (the larger the value of D, the higher the slope), the lag phase is modulated by the grid spacing *r*; the greater the lag phase, the longer *r* is (Figure 1). The spin diffusion build-up curve is simulated by varying either the distance *r* or the spin diffusion rate *D* and maintaining the other parameter constant.[7] For this reason, when comparing different *D* values (different samples) derived from the fit to *Eq. 1*, they all must be fitted using the same *r* value, and *vice versa*.

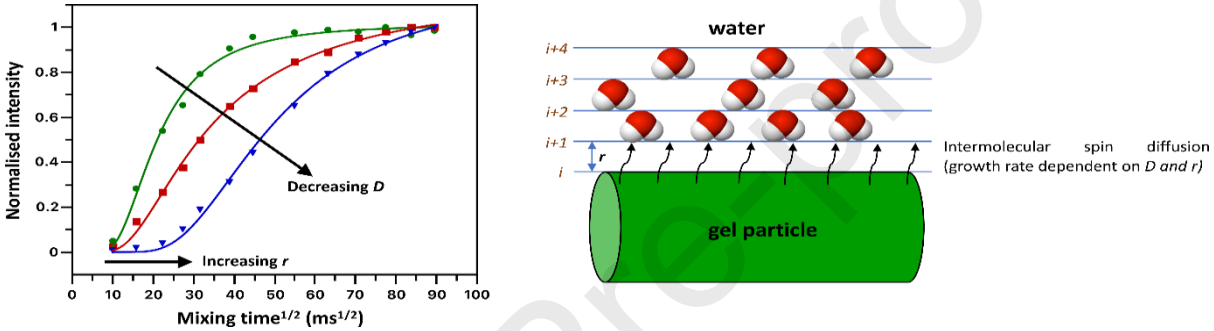


**Figure 1.** Schematic representation of the grid approximation of the spin diffusion model (right) and the influence of the parameters affecting the growth of the spin diffusion build-up curves (left).

Gels are two-component colloidal dispersions in which a gelator (solid continuous phase) is dispersed within a solvent (liquid dispersed phase).[11–13] Gels are typically constituted by 90-99 wt% of water and 1-10 wt% of solid particles of nm-to-µm size range.[1,5] Covalent or non-covalent interactions support continuous 3D gel network, with high quantities of solvent entrapped by capillary forces and surface tension.[3,4] In this heterogeneous system, the interplay of particle-particle and particle-solvent interactions defines the macroscopic properties of the material.[14–18] The role of the solvent is particularly difficult to characterise as different populations (e.g. free and bound) and microstructures (e.g. freezing and non-freezing) might coexist.[19] Also, protic solvents such as water can play the role of cross-linker of the particle network holding the gel structure (e.g. cellulose).[20] In a gel network constituted by charged particles (e.g. carboxymethylcellulose), the electric field around the ions can induce the water molecules constituting the ions hydration shells to rearrange into different structures.[21] Even though a direct correlation between changes in

the hydration shell of ions and gel swelling properties has not been reported, *Peppas and co-workers* observed a higher swelling ratio for copolymers with larger electrostatic repulsion.[22,23]

Recently, we reported on the use of STD NMR (in solution) to monitor residually protonated water (HDO) binding to particulate dispersions, and provided a detailed comparison of the strengths of this methodology with respect to classical NMR relaxation approaches.[17] To do this, we used TEMPO-oxidised cellulose dispersions (OCNF) in $D_2O$ as model systems.[17] The preparation of hydrogels in $D_2O$ allowed us to minimise the contribution of chemical exchange to the apparent STD factor of water, hence providing a more accurate estimation of the population of network-bound water. In particular, an increase of the STD factor of HDO at a specific saturation time was observed upon heating a diluted dispersion of OCNF, thus reporting an increased population of bound water. These data correlated with the enhanced solid-like behaviour measured by rheology.[17] This approach is valid when comparing STD factors for the gels with the same HDO and gelator concentrations. However, when comparing different sets of hydrogels prepared in $D_2O$, the final concentration of HDO depends on the chemical nature and concentration of the gelator and sample preparation (e.g. environmental humidity, sonication condition, etc.). Herein, we have extended the classical STD NMR analysis to monitor the structuration of water within different gels. We have carried out a systematic study on the experimental conditions affecting the apparent STD factor of the solvent in particulate dispersions. We have developed a novel STD NMR methodology, called Spin Diffusion Transfer Difference (SDTD), that is independent of gelator and solvent concentrations and can be accurately modelled using the classical 1D diffusion equation (Eq. 1). We demonstrate that the SDTD build-up curves (*i.e.* SDTD intensity *vs* square root of saturation time) enable the comparison of the degree of solvent structuration between different dispersions, hence allowing us to establish correlations between water structuration and the gel properties (e.g. stiffness). We show that the SDTD methodology can be applied to (i) the study of diluted dispersions (not possible by solid-state NMR spectroscopy) by solution NMR, and (ii) highly viscous gels using HR-MAS probes. As a proof of concept, we employed HR-MAS SDTD NMR to understand the role of the degree of structuration of cosolvents on the gelation properties of water/alcohol cellulose gels.

## 2. Materials and methods

### 2.1. Sample preparation

2.1.1. Gels prepared in $D_2O$

Dispersions of TEMPO-oxidised cellulose nanofibrils (OCNF), corn starch (CS) and enzymatically produced cellulose (EpC) at different concentrations were prepared in $D_2O$. OCNF of a degree of oxidation of ~ 25%, produced from purified softwood fibre and processed via high pressure homogenization, was kindly provided by Croda. These were further purified by dialysis against ultra-pure water (DI water, 18.2 MO cm) and stirred at room temperature for 30 min. Then the dispersion was acidified to pH 3 using HCl solution and dialysed against ultra-pure water (cellulose dialysis tubing MWCO 12400) for 3 days with the DI water replaced twice daily. The dialysed OCNF suspension was processed via mechanical shear (ULTRA TURRAX, IKA T25 digital, 30 minutes at 6500 rpm) and the pH was adjusted to 7 using NaOH solution. This dispersion was further dialysed to remove any remaining salts and dispersed using a sonication probe (Ultrasonic Processor, FB-505, Fisher), via a series of 1 s *on* 1 s *off* pulses for a net time of 60 min at 30% amplitude in an ice bath, and subsequently freeze-dried.

To prepare the OCNF dispersions for NMR investigation, OCNF powder and water were weighted to provide the desired weight concentrations of OCNF, and then probe sonicated for 30 min at 20% amplitude using pulses of 1 s *on* and 2 s *off,* using an ultrasonic processor vibracell VCX 130 sonicator. On the other hand, CS samples were first gelatinized in a boiling water bath for 30 minutes. The CS samples were sonicated for 2 min at 40% amplitude using 1 s *on* - 2 s *off* pulses.

For the $H_2O$ titration experiments, OCNF 1 wt% dispersions were prepared using MilliQ® water and $D_2O$ of 99.9 atom % D to achieve the desired $H_2O/D_2O$ ratio (5:95, 10:90, 20:80 and 30:70). For the variable gelator concentration experiments (OCNF and EpC at 0.5, 1 and 2 wt%), the samples were prepared by dilution from the 2 wt% dispersions to avoid error propagation.

2.1.2. OCNF 1 wt% cosolvent gels prepared in mixtures of $D_2O$ and alcohol-OD

First, stock dispersions of OCNF 2 wt% were prepared by redispersing OCNF powder in $D_2O$ by probe sonication for 1 min at 30% amplitude using 1 s *on* 1 s *off* pulses, using an ULTRA

TURRAX, IKA T25 digital sonicator. Subsequently, all the gels were prepared by dilution of the OCNF 2wt% dispersions using the corresponding alcohol-OD and $D_2O$ weight concentrations. $D_2O$ (151882) and 2-propanol-OD (615080) were purchased from Sigma-Aldrich. Ethanol-OD and methanol-OD were purchased from Cambridge Isotopes Lab, Inc.

**2.2. Nuclear magnetic resonance (NMR) spectroscopy**

Solution state NMR experiments were performed using a Bruker Avance I spectrometer equipped with a 5 mm triple resonance probe operating at frequency of 499.69 MHz ($^1$H). Saturation transfer difference (STD) NMR experiments of CS and OCNF dispersions were acquired at 298 K using a train of 50 ms Gaussian shaped pulses for selective saturation of the gelator particles, using an *on-resonance* frequency of 0 and -1 ppm for CS and OCNF dispersions, respectively, and an *off-resonance* frequency of 50 ppm. For the CS 15 wt% dispersion, saturation times ranging from 50 ms to 5 s were employed. For the experiments carried out on OCNF dispersions in water (*i.e.* $H_2O$ titrations and variable OCNF concentration), STD NMR experiments were performed using saturation times ranging from 100 ms to 8 s. A constant time length per scan (saturation time + recycle delay) of 8 s was used. Depending on saturation time, STD NMR experiments were performed with 128 scans or less (with a minimum of 16 scans), in inverse relation to the saturation time, and 8 dummy scans.

Variable concentration STD NMR experiments for EpC were carried out using a Bruker Avance II 800 MHz spectrometer equipped with a 5 mm inverse triple-resonance probe. The experiments were acquired at 298 K at saturation times ranging from 100 ms to 8 s, using a constant time length per scan (saturation time + recycle delay) of 8 s. The *on*- and *off*-resonance frequencies were set to -1 and 50 ppm, respectively. Depending on saturation time, STD NMR experiments were performed with 512 scans or less, in inverse relation to the saturation time, and 8 dummy scans.

The $D_2O$/alcohol-OD OCNF gels were characterised by high-resolution magic angle spinning (HR-MAS) using a solid-state Bruker Avance III spectrometer operating at a $^1$H frequency of 400.22 MHz with a triple resonance HR-MAS probe ($^1$H, $^{31}$P, $^{13}$C). All samples were spun at 6 kHz. HR-MAS NMR was required for these samples due to large $^1$H peak broadening precluding enough resolution in the absence of magic angle spinning. The large spectral broadening of the $D_2O$/alcohol-OD OCNF gels is due to their high viscosity leading to very

strong dipolar couplings, particularly for $D_2O$/ethanol-OD and $D_2O$/2-propanol-OD at high alcohol concentrations. To optimise the total experimental time for the acquisition of the STD NMR build-up curves for the 12 $D_2O$/alcohol-OD OCNF gels, the experiments were acquired by selective irradiation (*on*-resonance) of the $^1H$ peaks corresponding to OCNF surface domains (2.3-2.5 ppm) instead of core domains (*ca*. -1 ppm), and hence increasing the efficiency of the particle-to-solvent magnetisation transfer. A train of 50 ms Gaussian-shaped pulses were employed for saturation, with a field strength of 50 Hz.[24] STD NMR experiments using 0.5, 0.75, 1, 1.5, 2, 3, 4, 5, 6, 7 and 8 s saturation times were carried out, using a total relaxation time of 8.1 s. The *off*-resonance frequency was set to 56 ppm.

The STD spectra ($I_{STD}$) were obtained by subtracting the *on*- ($I_{sat}$) to the *off*-resonance ($I_0$) spectra. To determine the STD response or STD factor ($\eta_{STD}$), the peak intensities in the difference spectrum ($I_{STD}$) were integrated relative to the peak intensities in the *off*-resonance spectrum ($I_0$). The SDTD build-up curves were obtained by normalising all the STD factors against the highest value (usually corresponding to the longest saturation time).

<u>$T_1$ and $T_2$ relaxation experiments</u>

$^1H$ longitudinal relaxation times ($T_1$) were measured using a standard inversion recovery pulse sequence with a recycle delay of 5 s. 64 points were acquired at variable delay time after the inversion pulse, ranging from 25 ms to 50 s for OCNF, and 25 ms to 100 s for EpC.

The evolution of intensities of the HDO peak was fitted to the inversion-recovery monoexponential equation in TopSpin 4.1

$$M_z(\tau) = M_0\left[1 - 2e^{\left(-\frac{\tau}{T_1}\right)}\right] \qquad \textit{Eq. 2}$$

where $M_z$ is the z component of magnetisation, $M_0$the equilibrium magnetisation (at $\tau_\infty$), and $\tau$ the variable delay time. The additional factor of two arises as the recovery starts from inverted magnetization.

The Carr-Purcell-Meiboom-Gill (CPMG) experiment was carried out to determine the transversal relaxation time ($T_2$), using a recycle delay of 5 s. 64 points were acquired at variable spin echo period repetitions (40 µs per spin echo), so that the total evolution time ranged from 0.8 ms to 8 s. The relaxation of the HDO peak over the evolution time was fitted to the following monoexponential decay function

$$M_z(\tau) = M_0\left[e^{\left(-\frac{\tau}{T_2}\right)}\right] \qquad \textit{Eq. 3}$$

where $\tau$ is the refocusing time. The data were analysed using TopSpin 4.1 software.
The STD and SDTD graphs were generated using MATLAB.

### 2.3. Simulation of the SDTD build-up curves

To obtain a good fit of the SDTD buildup curve, it is essential to achieve a good sampling of both the lag phase and the plateau of the curve. To do so, using saturation times ranging from tens of milliseconds to 6-8 seconds is advised. The SDTD buildup curves were represented as a function of the square root of the saturation time and simulated in Matlab (Script 1) using *Eq.* 4. Here, the dependent variable is the normalized intensity of the NMR observable and the independent variable is the square root of the saturation time (in ms), *r* is the minimum distance of the grid (in nm), *D* is the spin diffusion rate (in $nm^2/ms$) at the particle/solvent interface, *erfc* is the complementary error function, *C* is the proportionally constant of the fit, and *b* is a parameter to centre the function around *x*. Notably, the growth rate of the SDTD curve presents a proportional and inversely proportional relationship to the spin diffusion rate *D* and the minimum distance *r*, respectively, both related to the degree of solvent structuration within the gel network. Hence, faster spin diffusion rates *D* and shorter distances *r* reflect increased solvent structuration.

## 3. Results and Discussion

### 3.1. Experimental validation of the 1D diffusion model to simulate SDTD NMR data

Particulate colloidal systems have been studied extensively by a combination of solution and solid-state NMR techniques.[6,17,25] For the investigation of internal dynamics and intermolecular interaction of particulate systems, solid-state NMR methods using polarization transfer and dipolar filtered pulse sequences are preferred and have been successfully employed to obtain topological information on the mode of interaction of membrane proteins to lipid bilayers, or the interactions of cellulose to matrix polysaccharides and water in plant cell walls.[5,6,26]

For very high molecular weight particles, the strength of anisotropic homonuclear dipolar couplings is high and, hence, the spin diffusion is very efficient and the principal mechanism of magnetisation transport through space. In fact, for melts of entangled polymers of high

molecular weight the "flip-flop" mechanism was shown to be predominant.[27] A similar situation is usually encountered for high molecular weight particles such as virus capsids[28,29] and carbohydrate particles, which have been traditionally studied in the solid or gel state by spin diffusion solid-state NMR methods.[6,26,30,31] On these grounds, we hypothesised that the kinetics of spin diffusion of large particles dispersed in solution (*i.e.* of very slow rotational and translational diffusion) can be modelled by *Eq. 1*.

The SDTD NMR method described in this work relies on the use of the 1D diffusion model (*Eq. 1*) to describe the transfer of magnetisation via spin diffusion from the rigid gel particle network to the mobile solvent phase. To do so, the STD NMR data are first normalised against the maximum apparent STD factor determined experimentally (typically the STD intensity at the longest saturation time employed), and then plotted against the square root of saturation time ($t_{sat}^{1/2}$). In addition, it is essential to sample the lag phase of the curve at very short saturation times to obtain a good fit of the SDTD equation. By substituting the *I* and *t* variables in *Eq. 1* with the SDTD factor and saturation time ($t_{sat}$), respectively, we obtain the SDTD curve (*Eq. 4*) as follows

$$SDTD = C \cdot erfc\left[\frac{r}{2 \cdot \sqrt{D \cdot t_{sat}}} - b\right] \qquad \textit{Eq. 4}$$

To experimentally validate that the interactions of a solvent with a particulate network can be modelled by *Eq. 4*, we monitored the evolution of the STD intensity with $t_{sat}$ for the HDO peak of two carbohydrate-based dispersions prepared in $D_2O$; in particular, a liquid-like TEMPO-oxidised cellulose (OCNF) 1 wt% dispersion (previously characterised in detail by rheology, NMR and SAXS)[17,32] and a corn starch (CS) 15 wt% gel (Figure 2, †ESI Figure S2). To sample the lag phase of the SDTD build-up curve, a saturation time as short as 50 ms was used (Figure 2). On the other hand, 8 s saturation time was necessary to reach the plateau of the curve for the OCNF 1 wt % dispersion (5 s was sufficient for the CS 15 wt% gel, Figure 2). The HDO SDTD build-up curve was then fitted using *Eq. 4* by keeping the grid spacing (r) constant to 2 Å, a value that has been reported for water-particle interfaces[8] (Figure 2). Also, the *b* parameter was kept constant and several values were tested to reach the best fit. In this regard, it should be noted that, as the parameter *D* is dependent on the *b* value used during the fit, only *D* values obtained from curve fits carried out using the same *b* can be compared. Thus, when comparing SDTD curves for which different *b* values provide the best fit, a compromise value must be chosen to determine *D*.

Comparison of the SDTD build-up curves of OCNF 1 wt% and CS 15 wt% shows faster spin diffusion growth at the CS-water interface (Figure 2, †ESI Table S1), indicating that, as expected, the degree of structuration of water is significantly higher in the viscous CS gel compared to the liquid-like OCNF dispersion.

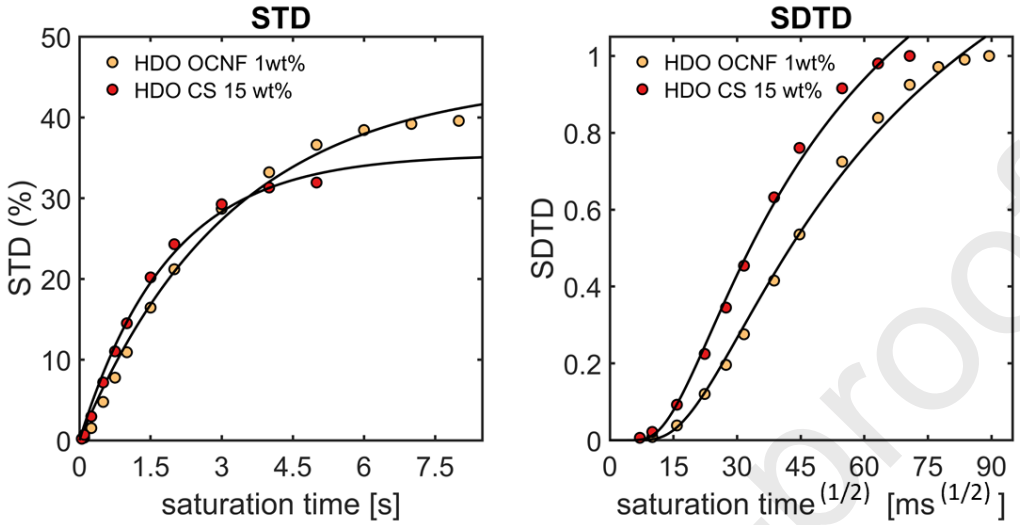


**Figure 2.** STD (left) and SDTD (right) build-up curves of the HDO peak for the OCNF 1 wt% dispersion (pale yellow) and corn starch (CS) 15 wt% gel (red) prepared in $D_2O$. The mathematical fits to *Eq. 4*, using a fixed grid spacing (*r*) of 2 Å, are shown. A *b* value of 1 was used for both SDTD curves.

### 3.2. The effect of solvent concentration on STD and SDTD build-up curves

To investigate the effect of solvent concentration on the SDTD build-up curve, we carried out $H_2O$ titrations to OCNF 1 wt% dispersions prepared in $D_2O$. Figure 3 shows the comparison of the STD vs SDTD build-up curves for HDO binding to OCNF particles for a broad range of water concentrations (below 0.1, 5, 10, 20 and 30 wt%). It is important to note that the STD factor is proportional to the fraction of ligand bound, *i.e.* the bound water ($f_{WB}$) in OCNF dispersions. Hence, at increasing $H_2O$ concentration the $f_{WB}$ decreases and, therefore, the STD factor decreases, as shown in Figure 3 - left. Notably, when we applied the SDTD methodology to these data, the effect of HDO concentration on the observed STD values was cancelled out, obtaining overlapping curves for all the HDO concentrations sampled (Figure 3 – right, †ESI Table S2). It should be noted that the ability to compensate for differences in HDO concentration when comparing different gels is essential, due to the extreme difficulty of maintaining the concentration of HDO under precise experimental control. Indeed, the HDO concentration in gels depends on (i) the $^2H$ purity of the batch of deuterated solvents used,

(ii) the relative humidity of the environment, and (iii) the solid content of the gel and the chemical structure of the gelator. The latter is particularly important for carbohydrate gels due to the high population of exchangeable protons in these materials.

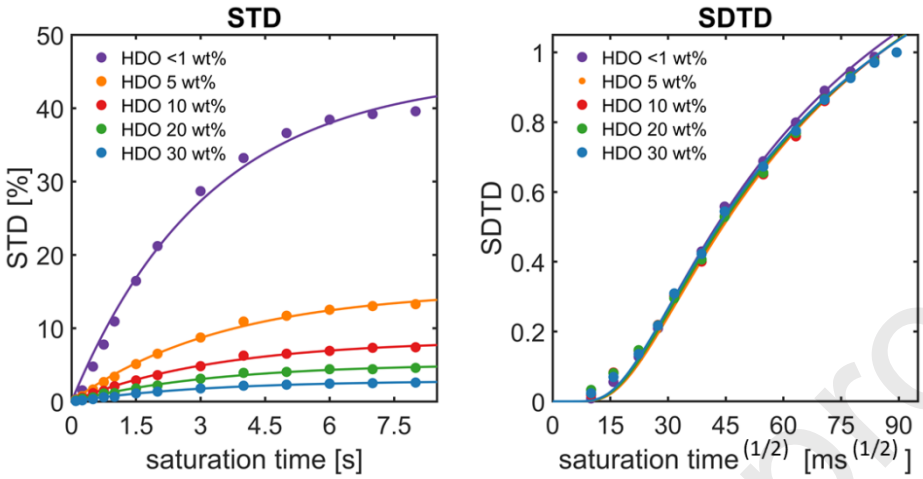


**Figure 3.** STD (left) and SDTD (right) build-up curves for HDO binding to OCNF 1 wt% dispersion acquired at different $H_2O/D_2O$ ratios. The $H_2O$ concentrations used go from < 0.1 wt% (purple), 5 wt% (yellow), 10 wt% (red), 20 wt% (green) and 30 wt% (light blue). A *b* value of 1 was used.

### 3.3. The effect of gelator concentration on STD and SDTD build-up curves: SDTD reports on changes in the degree of solvent structuration at the particle/solvent interface

As was mentioned above, the STD factor is strongly dependent on the fraction of bound solvent, and this is dependent on the concentration of gelator (*i.e.* the number of gelator binding sites available for the solvent to bind). In this regard, at higher gelator concentrations the fraction of bound solvent increases and, thus, the STD factor increases (Figure 4, left). Hence, the strong dependence of the STD build-up curve of the solvent on the concentration of gelator precludes the observation of changes in solvent structuration when comparing different gels. On the contrary, the SDTD factors are independent of solvent and gelator concentrations, hence allowing to monitor water structuration within gel networks with different gelator density. In this manuscript, by *solvent structuration* we refer to (i) the increased residence time and/or (ii) the reduced relative mobility, on average, of the network of bound solvent at the particle-solvent interface. Both scenarios would lead to enhanced spin diffusion transfer efficiency due to the increased anisotropic dipolar interactions, being the solvent in fast exchange.

To prove the effect of gelator concentration on the solvent SDTD build-up curves, we applied this method to study dispersions of neutral and negatively charged cellulose-like particles at different concentrations. First, we monitored enzymatically produced cellodextrin (EpC), which forms neutral particle networks. STD NMR experiments showed an increase of the STD factors at higher EpC concentrations. On the contrary, the SDTD build-up curves showed a perfect overlap for the three EpC concentrations tested (Figure 4a, †ESI Table S3), indicating that (i) solvent structure is not affected by EpC concentration, and (ii) the differences observed in the STD build-up curve are strictly due to changes in the fraction of bound solvent. Interestingly, when we carried out the same experiments for OCNF dispersions, the increase of gelator concentration resulted in a faster growth of both STD and SDTD build-up curves (Figure. 4b, †ESI Table S4). The faster SDTD build-up at higher OCNF concentration (*i.e.* increased D while keeping *r* and *b* constant; †ESI Table S4) reflects the more efficient spin diffusion transfer at the water-particle interface. This demonstrate that water becomes more structured upon increasing OCNF concentration (Figure 4b).

To interpret these results, it is key to consider the high density of negative charges present in OCNF (*ca*. 25 % of surface functionalisation), and the increased fibril-fibril overlap and association of $Na^+$ ions onto the fibrils at increasing OCNF concentration.[17] Thus, the increased degree of structuration of water at higher OCNF concentration might be due to (i) the formation of denser networks of structured water that shield the increasingly repulsive interactions between carboxylate groups, (ii) the increased presence of $Na^+$ ions onto the surface of OCNF fibrils leading to reduced fibril-fibril repulsion and, therefore, increased fibril-fibril overlap and water confinement, and (iii) the enhanced structuration of water around the $Na^+$ ions bound to the fibrils. However, as $Na^+$ is only present at stochiometric concentrations in our samples (very small compared to the HDO concentration), we expect a small contribution of the latter (point iii).

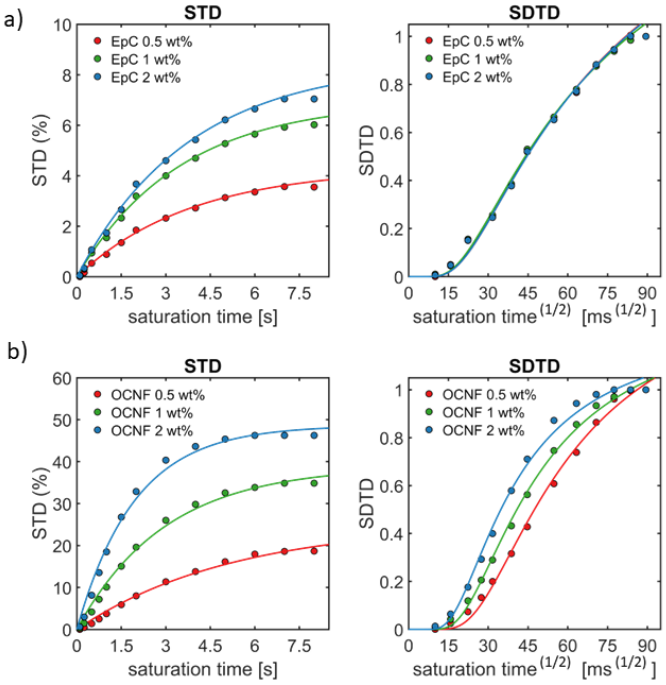


**Figure 4.** a) STD (left) and SDTD (right) build-up curves for HDO binding to EpC 0.5 wt% (light blue), 1 wt% (green) and 2 wt% (red) gels; b) STD (left) and SDTD (right) build-up curves for HDO binding to OCNF 0.5 wt% (light blue), 1 wt% (green) and 2 wt% (red) gels. A *b* values of 1 and 2 were used to obtain the best fit for the EpC and OCNF SDTD curves, respectively.

The determination of $T_1$ and $T_2$ relaxation times of HDO for the OCNF and EpC dispersions confirmed that the comparison of solvent relaxation times among different samples does not report consistently on differences in solvent structuration (†ESI Figure S3). Thus, HDO $T_2$ times decreased for both the EpC and OCNF samples at higher gelator concentrations, while SDTD NMR showed differences in HDO structuration for the OCNF dispersions only (†ESI Figure S3). Further, $T_1$ times decreased for the OCNF series and slightly increased for the EpC dispersions at the highest gelator concentration (†ESI Figure S3). Importantly, $T_1$ times higher than 7.9 s were measured for all samples and the faster OCNF-to-HDO spin diffusion transfer rates (*D*) at higher OCNF concentrations correlated with reduced HDO $T_1$ times. Hence, the determination of solvent structuration by SDTD NMR is not compromised by $T_1$ relaxation for the samples investigated herein.

### 3.4. SDTD NMR characterisation of the role of cosolvents on the alcohol-induced gelation of OCNF hydrogels: a case study

The alcohol-induced gelation of OCNF was recently investigated by rheology and SAXS.[33] Methanol, ethanol and 2-propanol (in order of decreasing hydrophilicity) were tested in their ability to induce OCNF gelation in mixtures with water. Alcohol hydrophilicity/hydrophobicity on its own did not explain the observed macroscopic properties. For example, methanol was able to induce gelation at the lowest concentration, followed by 2-propanol and ethanol. However, methanol and ethanol gels gave the weakest and stronger gels, respectively, at the point of gelation, while 2-propanol showed reduced stiffness compared to ethanol. With the exception of methanol gels, the analysis of SAXS data showed an increase in the cross-section of the OCNF nanofibrils above the gelation and phase separation concentrations.[33] The authors proposed that, having $Na^+$ preference for water over ethanol and 2-propanol (similar solubility of NaCl in methanol and water), gel formation could be driven to some extent by the aggregation of OCNF fibrils due to the increased association of $Na^+$ ions onto the surface of OCNF fibrils at higher ethanol and 2-propanol concentrations.[33] However, the difference in the solubility of NaCl in ethanol and methanol is not sufficiently large to explain the substantial differences of stiffness and fibril-fibril overlap in gels assembled in these alcohols (methanol gels are much weaker than ethanol gels), suggesting that other mechanisms must be involved. Thus, we hypothesised that water structuration must play an important role on gel properties.

To assess our hypothesis, we studied a series of OCNF gels prepared in cosolvent mixtures of water($D_2O$) and low molecular weight alcohols. The $D_2O$-exchanged alcohols methanol (MeOD), ethanol (EtOD) and 2-propanol (2PrOD) were studied at concentrations ranging from 10 to 60 wt% (see Materials and Methods section). An OCNF concentration of 1 wt% was used for all gels, and a dispersion of OCNF 1 wt% prepared in $D_2O$ was used as control sample.

Notably, the visual inspection of the SDTD curves clearly demonstrates the preferential binding of HDO to OCNF at all alcohol concentrations (much faster growth of the SDTD build-up curves of HDO compared to the alcohols; †ESI Figure S4). These results indicate that water constitutes the first solvation shell(s) of OCNF nanofibrils, while the alcohol component would only establish indirect interactions mediated by water.

Aiming to monitor the degree of structuration of HDO before, during and after gelation (*i.e.* upon addition of increasing concentrations of alcohol), we calculated the spin diffusion rate

*D* of HDO for each water/alcohol gel (Figure 5a-c, †ESI Table S5-S7), and normalised it against the spin diffusion rate $D_0$ of HDO for the control sample without alcohol (OCNF 1 wt% in $D_2O$, Figure 2 - left). Thus, the $D/D_0$ ratio of HDO was plotted as a function of alcohol content (Figure 5d). Firstly, it should be noted the lower $D/D_0$ values for the MeOD compared to the EtOD and 2PrOD gels above the point of gelation. Also, MeOD gels showed a significant $D/D_0$ decrease up to 30 wt% followed by an increase up to the $D/D_0$ value of 1 (*i.e.* very similar to the control sample) at 60 wt% of MeOD (no syneresis observed at this concentration). This suggest a lower capacity of MeOD to induce water structuration in OCNF gels compared to EtOD and 2PrOD, which correlates with previous SAXS studies showing that the cross-section and overlap of OCNF fibrils do not vary significantly with methanol concentration.[33]

On the other hand, ethanol gels showed a continuous increase of $D/D_0$ upon gelation (30 wt% of ethanol) and up to 60 wt% of alcohol content, while the D of ethanol was not affected significantly (Figure 5d, point of syneresis indicated with a star). This means that the degree of structuration of water within the gel network increases with ethanol concentration, which correlates to the ethanol-induced increase of the average OCNF fibril cross-section (*i.e.* increase of fibril-fibril overlap), whereas the structuration of ethanol is barely affected. This further confirms that ethanol does not interact directly with the OCNF network, but possibly forms microdomains similar to what was described before for the mechanism of alcohol-induced gelation of clays.[34] Regarding 2-propanol gels, a behaviour very similar to ethanol gels was observed above 30 wt% of 2-propanol, although no significant differences of $D/D_0$ were observed for concentrations below 30 wt%.

Our SDTD NMR approach highlights the essential role of water structuration on the gelation properties of OCNF gels prepared in water and low molecular weight alcohol mixtures. In particular, the higher stiffness of water/ethanol and water/2-propanol gels correlates with their best ability to form networks of highly structured water compared to water/methanol gels, most likely due to the increased water confinement within the denser OCNF particle network (increased OCNF particle cross-section).[33] On the other hand, ethanol and 2-propanol could organise into microdomains due to the more favourable water-water and alcohol-alcohol compared to water-alcohol interactions. Notably, a similar mechanism was proposed for the alcohol-induced gelation of clays, where the clay particles were also in the sodium-salt form.[34] Overall, the SDTD NMR method has provided important new insights on the molecular features governing the mechanism of gelation and macroscopic properties

of ONCF water/alcohol gels. We demonstrate that, besides fibril-fibril overlap and NaCl solubility in the alcohols, the degree of water structuration also plays a critical role on gel properties.

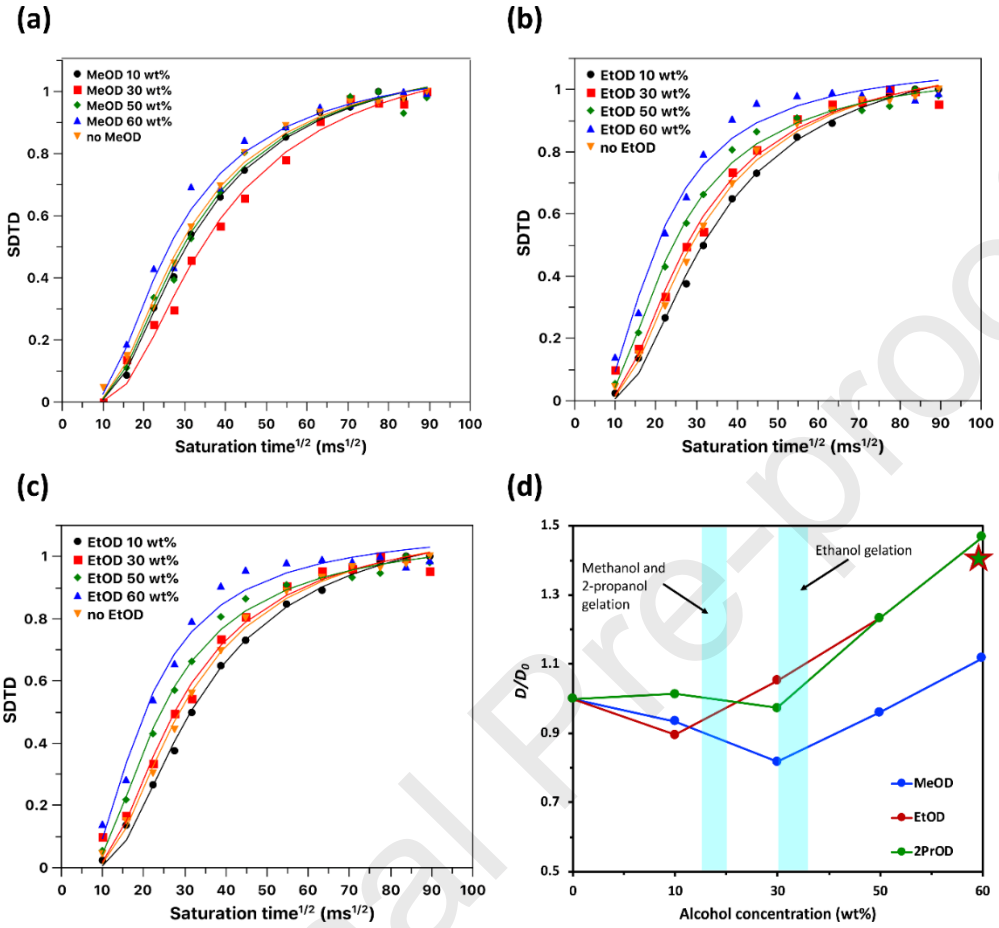


**Figure 5.** SDTD NMR build-up curves of the HDO peak in OCNF 1 wt% gels prepared in $D_2O$/MeOD (**a**) $D_2O$/EtOD (**b**) and $D_2O$/2PrOD (**c**) cosolvent mixtures. The SDTD curve for the control sample (OCNF 1 wt% in 100% $D_2O$, 0% alcohol), is shown in orange. The SDTD curves for the $D_2O$/alcohol-OD gels are shown in black (10 wt% of alcohol-OD), red (30 wt% of alcohol-OD), green (50 wt% of alcohol-OD), and blue (60 wt% of alcohol-OD). A *b* value of 2 was used for all curves. (**d**) Plot showing the evolution of the normalised spin diffusion rate ($D/D_0$) of HDO binding to OCNF 1 wt% containing different concentrations of MeOD, EtOD and 2PrOD. $D_0$ represents the value of D of HDO calculated in the absence of alcohol (OCNF 1 wt% in $D_2O$, control sample). The *D* value of HDO in each water-alcohol gel sample was obtained from the fit of the SDTD build-up curves shown in (**a**), (**b**) and (**c**). The ranges of alcohol concentrations leading to gelation are shown as cyan areas. The concentration (*ca*. 60 wt%) at which phase separation occurs for ethanol and 2-propanol gels is indicated with a star.

## 4. Conclusions

The NMR investigation of the structure and dynamics of solvents have traditionally relied on the determination of $^1H$ $T_1$ and $T_2$ relaxation times.[35,36] However, while $T_1$ relaxation times can be ambiguous (high $T_1$ times might indicate either very fast or very slow dynamics), $T_2$ relaxation is strongly affected by the kinetics of chemical exchange, obscuring the effect of molecular motion and, therefore, hindering the characterisation of solvent structuration. In addition, $T_1$ and $T_2$ relaxation measurements do not allow for the direct observation of free and bound populations for fast-exchanging solvents, providing average values over the total number of solvent molecules instead (Table 1). This precludes the unambiguous comparision of solvation properties among different gel preparations. On the other hand, Pulsed Gradient Spin-Echo (PGSE) NMR experiments[37] have been applied to the determination of the molecular self-diffusion coefficient of solvents, important to characterise the dynamics of solvent exchange or mesh swelling and deswelling processes,[38] among others; however, PGSE does not allow for the direct observation of the spin diffusion transfer at the particle/solvent interface (Table 1). Beyond the NMR field, x-ray and neutron diffraction techniques have been applied to the study of solvent dynamics;[19,39] nonetheless, these techniques also lack interfacial resolution and require the singular equipment and expertise available at national facilities only.[19]

Following previous appications of the classical STD NMR approach for the monitorisation of solvent and small ligand interactions to dispersions of particulate networks,[17,40,41] we have notably extended the applicability of this ligand-observed NMR technique to overcome the limitations of the classical approach; this is, (i) STD NMR reports on the fraction of bound solvent but does not inform on water structuration, and (ii) STD intensities are strongly dependent on solvent and gelator concentrations, hence precluding the comparison of solvation properties between diffent colloidal dispersions (Table 1). We have validated our initial hypothesis stating that, under conditions of negligible translational diffusion of the receptor molecule within the NMR time scale (*i.e.* for large particles), (i) the particle-to-solvent spin diffusion transfer can be monitored by performing STD NMR experiments at varying saturation times followed by normalisation against the maximum STD intensity registered at long saturation times, which yields the SDTD build-up curve, (ii) the SDTD curves can be modelled using the general 1D diffusion equation (Figure 2) and are

exclusively dependent on the minimum receptor-to-solvent distance (*r*) and the receptor-to-solvent spin diffusion rate (*D*) at the particle/solvent interface (Eq. 4), and (iii) only changes in solvent structuration can give rise to different *D* values (e.g different types of particle networks or different concentrations of surface charged gelator leading to rearrangements of the gel netowrk; Figure 6).

To our knowledge, the SDTD NMR protocol described herein constitutes the first ligand-observed solution NMR method allowing the quantitative characterisation of the degree of solvent(s) structuration at the particle/solvent interface (e.g. related to the size of structured solvent networks or number of solvation shells). Notably, it presents an important advantage over solid-state NMR experiments[5,6] based on the same spin diffusion principles such as the water polarization transfer (WPT) NMR experiment; thus, while the SDTD approach relies on monitoring the well-resolved solvent peaks by solution or HR-MAS NMR, WPT monitors the broad or frequently invisible particle peak, requires the more specialised solid-state NMR setup (Table 1), and relies on the cross-polarisation efficiency and the observation of low abundant nuclei. Further, SDTD NMR allows for the study of diluted dispersions, not possible by WPT solidstate NMR experiments, as well as highly viscous gels using an HR-MAS probe.

Table 1. Comparison of the different NMR techniques that have been employed to characterise solvent properties. Y: yes; N: no. The SDTD protocol stands out by its simplicity, independence on solvent and gelator concentrations, interfacial and ligand-observed nature and dependence on water structuration at the particle/solvent interface.

| | **Relaxation NMR** | **PGSE NMR** | **WPT CP** (solid-state NMR) | **STD** | **SDTD** |
|---|---|---|---|---|---|
| **Depends on solvent concentration** | Y | Y | N | Y | **N** |
| **Depends on gelator concentration** | Y | Y | N | Y | **N** |
| **Direct observation of bound solvent** | N | N | Y | Y | Y |
| **Reports on solvent structuration** | N | N | Y | N | **Y** |
| **Direct observation of the gelator/solvent interface** | N | N | Y | Y | **Y** |

| | | | | | |
|---|---|---|---|---|---|
| **Solvent-observed technique** | Y | Y | N | Y | **Y** |
| **Accessibility and ease of use** | High | Medium | Low | High | **High** |

Further, the application of the SDTD protocol to OCNF-water/alcohol gels previously characterised by scattering and rheological approaches enabled the understanding of the role the cosolvents on the macroscopic properties of these materials. The SDTD build-up curves demonstrated that (i) water binds preferentially to OCNF over any of the three alcohols tested (methanol, ethanol and 2-propanol), and (ii) the degree of water structuration increases with alcohol concentration for the water/ethanol and water/2-propanol gels. This effect correlates to the much higher gel strength of water/ethanol and water/2-propanol gels compared to methanol gels. [33]

We have demonstrated that the applicability of STD NMR can be extended beyond its traditional boundaries for very high molecular weight receptors such as carbohydrate particles. The novel SDTD approach will provide the community of scientists dealing with colloids and interfaces with a straightforward, fast and robust ligand-observed NMR technique to quantitatively characterise role of solvent(s) organisation on the mechanisms of gelation and the macroscopic properties of a wide range of colloidal particulate materials. Further, we believe that future applications of the SDTD method to the evaluation and classification of organ/tissue integrity and stability present might benefit the biological and clinical areas.

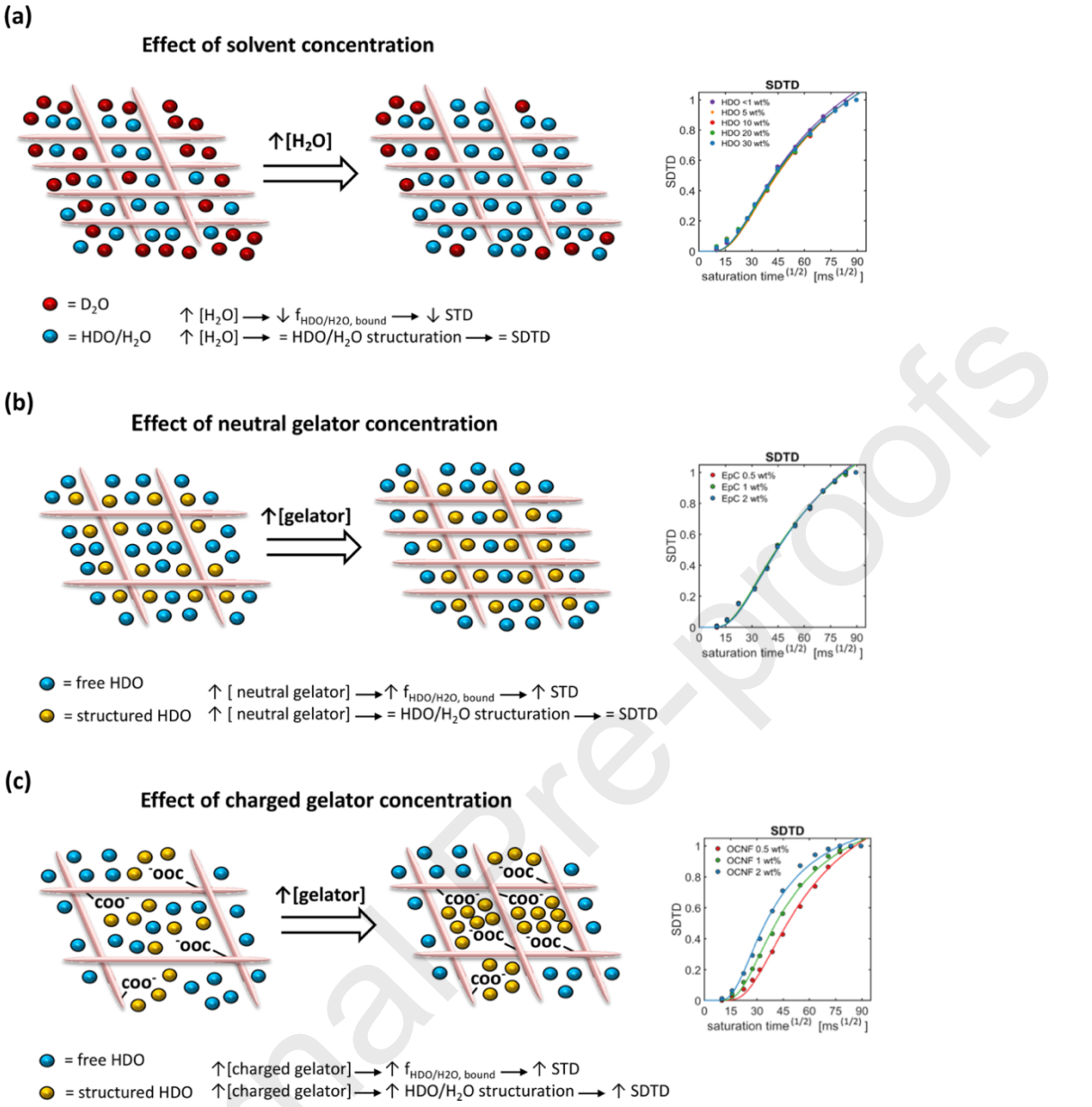


**Figure 6.** Summary of the main findings reported in this article. The effect of solvent (a) and gelator concentration, for neutral (b, EpC) and charged (c, OCNF) gelators, on the SDTD build-up curves and the degree of structuration of water within the gel network is shown.

## Author information

### Corresponding Authors

* Correspondence should be addressed to Yaroslav Z. Khimyak (y.khimyak@uea.ac.uk), Juan C. Muñoz García (j.munoz-garcia@uea.ac.uk) and Ridvan Nepravishta (rineprav@utmb.edu)

### Present Addresses

†If an author's address is different than the one given in the affiliation line, this information may be included here.

**Author Contributions**

The manuscript was written through contributions of all authors. All authors have given approval to the final version of the manuscript.

**Funding Sources**

This work was funded through the Innovate UK Project: Enzymatically Produced Interpenetrating Gels of Cellulose and Starch, via the EPRSC/Innovate UK grant IUK 59000 442149 (UEA) and EPSRC grants EP/N033337/1 (UEA) and EP/N033310/1 (University of Bath).

**Notes**

The authors declare no competing financial interest. In the Electronic Supporting Information, we include the Matlab and Python scripts to plot and fit the SDTD build-up curves.

## Acknowledgments

We thank the GelEnz consortium, which is funded by EPSRC (Grant Research Number: IUK 59000 442149). The Engineering and Physical Sciences Research Council (EPSRC) is acknowledged for provision of financial support (EP/N033337/1) for J.C.M.G., J.A. and Y.Z.K. and (EP/N033310/1) for M.A.d.S and K.J.E. R.N acknowledges financial support from BBSRC (grant BB/P010660/1). We are also grateful for UEA Faculty of Science NMR facility. V.G. would like to acknowledge the support of BBSRC Norwich Research Park Bioscience Doctoral Training Grant (BB/M011216/1). Additional research data supporting this publication are available as electronic supplementary files at the DOI:xxx.

## References

[1] N. Bloembergen, On the interaction of nuclear spins in a crystalline lattice, Physica. 15 (1949) 386–426. https://doi.org/10.1016/0031-8914(49)90114-7.

[2] L. Emsley, Spin Diffusion for NMR Crystallography, Encycl. Magn. Reson. (2009). https://doi.org/10.1002/9780470034590.emrstm1010.

[3] A. Kubo, C.A. McDowell, Spectral spin diffusion in polycrystalline solids under magic-angle spinning, J. Chem. Soc. Faraday Trans. 1 Phys. Chem. Condens. Phases. 84 (1988) 3713–3730. https://doi.org/10.1039/F19888403713.

[4] B.H. Meier, Polarization Transfer and Spin Diffusion in Solid-State NMR, Adv. Magn. Opt.

Reson. 18 (1994) 1–116.

[5] D. Huster, X. Yao, M. Hong, Membrane protein topology probed by 1H spin diffusion from lipids using solid-state NMR spectroscopy, J. Am. Chem. Soc. 124 (2002) 874–883. https://doi.org/10.1021/ja017001r.

[6] P.B. White, T. Wang, Y.B. Park, D.J. Cosgrove, M. Hong, Water-polysaccharide interactions in the primary cell wall of arabidopsis thaliana from polarization transfer solid-state NMR, J. Am. Chem. Soc. 136 (2014) 10399–10409. https://doi.org/10.1021/ja504108h.

[7] R. Mani, S.D. Cady, M. Tang, A.J. Waring, R.I. Lehrer, M. Hong, Membrane-dependent oligomeric structure and pore formation of a β-hairpin antimicrobial peptide in lipid bilayers from solid-state NMR, Proc. Natl. Acad. Sci. 103 (2006) 16242–16247. https://doi.org/10.1073/pnas.0605079103.

[8] K.K. Kumashiro, K. Schmidt-Rohr, O.J. Murphy, K.L. Ouellette, W.A. Cramer, L.K. Thompson, A Novel Tool for Probing Membrane Protein Structure: Solid-State NMR with Proton Spin Diffusion and X-Nucleus Detection, J. Am. Chem. Soc. 120 (1998) 5043–5051. https://doi.org/10.1021/ja972655e.

[9] J. Clauss, K. Schmidt-Rohr, H.W. Spiess, Determination of domain sizes in heterogeneous polymers by solid-state NMR, Acta Polym. 44 (1993) 1–17. https://doi.org/10.1002/actp.1993.010440101.

[10] J. Wang, On the determination of domain sizes in polymers by spin diffusion, J. Chem. Phys. 104 (1996) 4850–4858. https://doi.org/10.1063/1.471179.

[11] D.H. Everett, Basic Principles of Colloid Science, The Royal Society of Chemistry, 1988. https://doi.org/10.1039/9781847550200.

[12] P.C. Marr, A.C. Marr, Ionic liquid gel materials: applications in green and sustainable chemistry, Green Chem. 18 (2016) 105–128. https://doi.org/10.1039/C5GC02277K.

[13] M. Bender, The colloidal state, Am. Sci. 46 (1958) 368–387. http://www.jstor.org/stable/27827200.

[14] M. Martínez-Sanz, M.J. Gidley, E.P. Gilbert, Hierarchical architecture of bacterial cellulose and composite plant cell wall polysaccharide hydrogels using small angle neutron scattering, Soft Matter. 12 (2016) 1534–1549. https://doi.org/10.1039/c5sm02085a.

[15] S. Park, J.O. Baker, M.E. Himmel, P.A. Parilla, D.K. Johnson, Cellulose crystallinity index: Measurement techniques and their impact on interpreting cellulase performance, Biotechnol. Biofuels. 3 (2010) 10. https://doi.org/10.1186/1754-6834-3-10.

[16] A.Y. Abuelfilat, Y. Kim, P. Miller, S.P. Hoo, J. Li, P. Chan, J. Fu, Bridging structure and mechanics of three-dimensional porous hydrogel with X-ray ultramicroscopy and atomic

force microscopy, RSC Adv. 5 (2015) 63909–63916. https://doi.org/10.1039/c5ra10942f.

[17] V. Calabrese, J.C. Muñoz-García, J. Schmitt, M.A. da Silva, J.L. Scott, J. Angulo, Y.Z. Khimyak, K.J. Edler, Understanding heat driven gelation of anionic cellulose nanofibrils: Combining saturation transfer difference (STD) NMR, small angle X-ray scattering (SAXS) and rheology, J. Colloid Interface Sci. 535 (2019) 205–213. https://doi.org/10.1016/j.jcis.2018.09.085.

[18] J.C. Muñoz-García, K.R. Corbin, H. Hussain, V. Gabrielli, T. Koev, D. Iuga, A.N. Round, D. Mikkelsen, P.A. Gunning, F.J. Warren, Y.Z. Khimyak, High Molecular Weight Mixed-Linkage Glucan as a Mechanical and Hydration Modulator of Bacterial Cellulose: Characterization by Advanced NMR Spectroscopy, Biomacromolecules. 20 (2019) 4180–4190. https://doi.org/10.1021/acs.biomac.9b01070.

[19] H. O'Neill, S.V. Pingali, L. Petridis, J. He, E. Mamontov, L. Hong, V. Urban, B. Evans, P. Langan, J.C. Smith, B.H. Davison, Dynamics of water bound to crystalline cellulose, Sci. Rep. 7 (2017) 11840. https://doi.org/10.1038/s41598-017-12035-w.

[20] I. Jankowska, R. Pankiewicz, K. Pogorzelec-Glaser, P. Ławniczak, A. Łapiński, J. Tritt-Goc, Comparison of structural, thermal and proton conductivity properties of micro- and nanocelluloses, Carbohydr. Polym. 200 (2018) 536–542. https://doi.org/https://doi.org/10.1016/j.carbpol.2018.08.033.

[21] Y. Marcus, Effect of Ions on the Structure of Water: Structure Making and Breaking, Chem. Rev. 109 (2009) 1346–1370. https://doi.org/10.1021/cr8003828.

[22] R. Barbucci, A. Magnani, M. Consumi, Swelling Behavior of Carboxymethylcellulose Hydrogels in Relation to Cross-Linking, pH, and Charge Density, Macromolecules. 33 (2000) 7475–7480. https://doi.org/10.1021/ma0007029.

[23] F. Madsen, N.A. Peppas, Complexation graft copolymer networks: swelling properties, calcium binding and proteolytic enzyme inhibition, Biomaterials. 20 (1999) 1701–1708. https://doi.org/https://doi.org/10.1016/S0142-9612(99)00071-X.

[24] M. Mayer, B. Meyer, Characterization of ligand binding by saturation transfer difference NMR spectroscopy, Angew. Chemie - Int. Ed. 38 (1999) 1784–1788. https://doi.org/10.1002/(SICI)1521-3773(19990614)38:12<1784::AID-ANIE1784>3.0.CO;2-Q.

[25] R. Dupree, T.J. Simmons, J.C. Mortimer, D. Patel, D. Iuga, S.P. Brown, P. Dupree, Probing the molecular architecture of arabidopsis thaliana secondary cell walls using two- and three-dimensional 13C solid state nuclear magnetic resonance spectroscopy, Biochemistry. 54 (2015) 2335–2345. https://doi.org/10.1021/bi501552k.

[26] T. Wang, M. Hong, Solid-state NMR investigations of cellulose structure and interactions with matrix polysaccharides in plant primary cell walls, J. Exp. Bot. 67 (2016) 503–514.

https://doi.org/10.1093/jxb/erv416.

[27] N.F. Fatkullin, G.A. Yatsenko, R. Kimmich, E. Fischer, Theory of spin diffusion in liquid-phase polymer systems, J. Exp. Theor. Phys. 87 (1998) 294–302. https://doi.org/10.1134/1.558659.

[28] E. Barbet-Massin, M. Felletti, R. Schneider, S. Jehle, G. Communie, N. Martinez, M.R. Jensen, R.W.H. Ruigrok, L. Emsley, A. Lesage, M. Blackledge, G. Pintacuda, Insights into the Structure and Dynamics of Measles Virus Nucleocapsids by 1H-detected Solid-state NMR, Biophys. J. 107 (2014) 941–946. https://doi.org/https://doi.org/10.1016/j.bpj.2014.05.048.

[29] P.C. Magusin, M.A. Hemminga, 2D exchange 31P NMR spectroscopy of bacteriophage M13 and tobacco mosaic virus, Biophys. J. 68 (1995) 1128–1136. https://doi.org/https://doi.org/10.1016/S0006-3495(95)80287-0.

[30] M. Foston, R. Katahira, E. Gjersing, M.F. Davis, A.J. Ragauskas, Solid-State Selective 13C Excitation and Spin Diffusion NMR To Resolve Spatial Dimensions in Plant Cell Walls, J. Agric. Food Chem. 60 (2012) 1419–1427. https://doi.org/10.1021/jf204853b.

[31] T. Wang, J.K. Williams, K. Schmidt-Rohr, M. Hong, Relaxation-compensated difference spin diffusion NMR for detecting 13C–13C long-range correlations in proteins and polysaccharides, J. Biomol. NMR. 61 (2015) 97–107. https://doi.org/10.1007/s10858-014-9889-0.

[32] J. Schmitt, V. Calabrese, M.A. da Silva, S. Lindhoud, V. Alfredsson, J.L. Scott, K.J. Edler, TEMPO-oxidised cellulose nanofibrils; probing the mechanisms of gelation via small angle X-ray scattering, Phys. Chem. Chem. Phys. 20 (2018) 16012–16020. https://doi.org/10.1039/C8CP00355F.

[33] M.A. da Silva, V. Calabrese, J. Schmitt, D. Celebi, J.L. Scott, K.J. Edler, Alcohol induced gelation of TEMPO-oxidized cellulose nanofibril dispersions, Soft Matter. 14 (2018) 9243–9249. https://doi.org/10.1039/C8SM01815D.

[34] Y. Kimura, K. Haraguchi, Clay–Alcohol–Water Dispersions: Anomalous Viscosity Changes Due to Network Formation of Clay Nanosheets Induced by Alcohol Clustering, Langmuir. 33 (2017) 4758–4768. https://doi.org/10.1021/acs.langmuir.7b00764.

[35] Y.E. Shapiro, Structure and dynamics of hydrogels and organogels: An NMR spectroscopy approach, Prog. Polym. Sci. 36 (2011) 1184–1253. https://doi.org/10.1016/j.progpolymsci.2011.04.002.

[36] C.L. Cooper, T. Cosgrove, J.S. Van Duijneveldt, M. Murray, S.W. Prescott, The use of solvent relaxation NMR to study colloidal suspensions, Soft Matter. 9 (2013) 7211–7228. https://doi.org/10.1039/c3sm51067k.

[37] W.S. Price, NMR Studies of Translational Motion: Principles and Applications., Cambridge University Press, 2009.

[38] P. Porion, E. Ferrage, F. Hubert, E. Tertre, T. Dabat, A.M. Faugère, F. Condé, F. Warmont, A. Delville, Water Mobility within Compacted Clay Samples: Multi-Scale Analysis Exploiting 1H NMR Pulsed Gradient Spin Echo and Magnetic Resonance Imaging of Water Density Profiles, ACS Omega. 3 (2018) 7399–7406. https://doi.org/10.1021/acsomega.8b01083.

[39] K. Amann-Winkel, M.-C. Bellissent-Funel, L.E. Bove, T. Loerting, A. Nilsson, A. Paciaroni, D. Schlesinger, L. Skinner, X-ray and Neutron Scattering of Water, Chem. Rev. 116 (2016) 7570–7589. https://doi.org/10.1021/acs.chemrev.5b00663.

[40] S.M. Ramalhete, K.P. Nartowski, N. Sarathchandra, J.S. Foster, A.N. Round, J. Angulo, G.O. Lloyd, Y.Z. Khimyak, Supramolecular Amino Acid Based Hydrogels: Probing the Contribution of Additive Molecules using NMR Spectroscopy, Chem. - A Eur. J. 23 (2017) 8014–8024. https://doi.org/10.1002/chem.201700793.

[41] M. Wallace, J.A. Iggo, D.J. Adams, Probing the surface chemistry of self-assembled peptide hydrogels using solution-state NMR spectroscopy, Soft Matter. 13 (2017) 1716–1727. https://doi.org/10.1039/C6SM02404A.

## CRediT author statement

**Valeria Gabrielli:** Formal Analysis, Investigation, Data Curation, Writing – Original Draft, Visualization. **Agne Kuraite**: Formal Analysis, Investigation, Visualization. **Marcelo Alves da Silva**: Investigation, Writing – Review & Editing. **Karen J. Edler**: Resources, Writing – Review & Editing, Supervision, Funding Acquisition. **Jesús Angulo**: Resources, Writing – Review & Editing, Supervision, Funding Acquisition. **Ridvan Nepravishta:** Conceptualization, Methodology, Data Curation, Writing – Original Draft, Writing – Review & Editing, Visualization, Supervision. **Juan C. Muñoz-García**: Conceptualization, Methodology, Data Curation, Writing – Original Draft, Writing – Review & Editing, Visualization, Supervision. **Yaroslav Z. Khimyak**: Resources, Writing – Review & Editing, Supervision, Funding Acquisition.

## Declaration of interests

☒ The authors declare that they have no known competing financial interests or personal relationships that could have appeared to influence the work reported in this paper.

☐The authors declare the following financial interests/personal relationships which may be considered as potential competing interests: